Input-to-State Robustness Control for Human–Cable Interaction in Cable-Driven Parallel Robots

Ridvan Keskin[1], Hanbang Gao[2,3], Christine Chevallereau[2], Stéphane Caro[2]

***Abstract*— This paper addresses safe, accurate control of cable-driven parallel robots (CDPRs) during human–cable interaction, where unilateral cable constraints and contact-induced disturbances make closed-loop stability and oscillation challenging. Therefore, we propose a rapidly exponential input to state stabilizing control Lyapunov functions (RES–ISS–CLF) controller that provides input-to-state stability guarantees under external wrench on the robot. To mitigate human–cable collisions, we augment the control law with a quadratic programming (QP)-based tension distribution algorithm that constraints the upper bound of the cable with a time-varying function while preserving feasibility. A wrapping simulator with a fixed cylinder emulating an arm-like obstacle is modeled to reproduce the human-cable interaction scenario. The proposed method achieves solid trajectory tracking performance and ensures the stability of the control system. The performance of the control law is compared with a PID and CLF-QP controllers. The method unifies exponential stability with hard constraint enforcement and practical collision handling, especially during contact and recovery.**

***Index Terms*— Cable-Driven Parallel Robots, physical human–robot interaction, collision management, control Lyapunov function, quadratic programming, input-to-state stability.**

I. Introduction

Cable-Driven Parallel Robots (CDPRs) are parallel manipulators whose moving platform (MP) is actuated by unidirectional tension cables rather than rigid links. These characteristics confer high reconfigurability, large workspaces, and high payload-to-mass ratios, leading to deployments across industrial handling, entertainment, and construction [1], [2]. At the same time, cables can only pull, not push. They can sag, and their wrapping through space couples geometry, constraints, and dynamics. These features make closed-loop control and safety assurance non-trivial in human–robot collaboration (HRC) scenarios.

The high reconfiguration of CDPRs has hindered the establishment of standardized, off-the-shelf collaborative components and procedures [3], [4]. Beyond this lack of standardization, modeling errors remain a first-order concern: geometric misplacement, pulley and routing simplifications, cable elongation and sag, and sensing biases all degrade pose estimation and tracking accuracy [5]–[7]. Dynamic uncertainties compound the problem. Nonlinear and rate-dependent cable stiffness and hysteresis, friction, and varying inertial properties are hard to identify and to maintain across operating conditions [8], [9]. To cope, the literature explores adaptive and robust strategies (e.g., adaptive dynamics, sliding-mode variants) [10]–[12]. It also investigates data-driven and optimization schemes (e.g., deep RL, MPC) that reduce reliance on exact priors [13], [14]. Nevertheless, no single approach ensures formal stability while simultaneously enforcing unilateral cable constraints during contact-rich interactions.

In shared workspaces, CDPR cables may contact around human limbs or environmental objects as shown in Fig. 1. Such cable–environment interference can create abrupt tension rises and impulsive loads if not detected and mitigated quickly [15]. Cable–cable interference further perturbs kinematics and can induce jerky motion or sudden releases [16]. Because humans can deviate the MP from planned paths, interference likelihood increases during pHRI. Safe collaboration, therefore, demands controllers that enforce unilateral tension constraints. They must manage tensions proactively during collision and wrapping, and also preserve tracking without exciting oscillations.

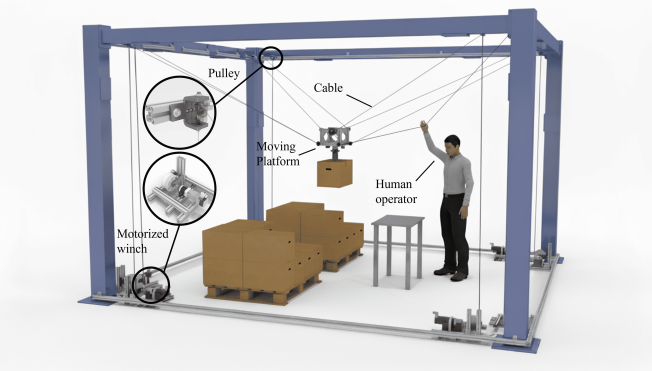

Fig. 1. Human-cable physical contact in the shared workspace

Recent frameworks have introduced end-to-end pipelines for human–cable collision handling in CDPRs, including detection, cable identification, online management, and end-of-collision recovery [17]. Subsequent work extended these frameworks to incorporate cable length and trajectory tracking during collisions, as well as to address broader carrying tasks involving multiple contact types and contact distinction [18], [19]. In these works, tension reduction during human–cable collision is typically achieved via PID-based corrections combined with sequential tension upper-bound

Corresponding author: hanbang.gao@ls2n.fr.

[1] Electrical and Electronics Engineering, Zonguldak Bulent Ecevit University, Zonguldak, 67100 Türkiye. E-mail: {ridvan.keskin}@beun.edu.tr

[2]Nantes Université, École Centrale de Nantes, CNRS, LS2N, UMR 6004, 44000 Nantes, France. Email: {hanbang.gao, christine.chevallereau, stephane.caro}@ls2n.fr

[3]Department of Mechanical and Production Engineering, Nantes Université, IUT de Nantes, 44300 Nantes, France.

schedules. While effective in practice, these strategies lack a closed-loop stability analysis and do not explicitly dissipate the excess energy that causes post-collision oscillations [19].

Control Lyapunov Function–Quadratic Programming (CLF–QP) approaches for CDPRs demonstrate principled tracking design [20], and Lyapunov-based analyses exist for synchronous impedance control of MP–environment interactions [21]. However, these lines typically target nominal operation or MP contacts, not human–cable collisions. The methods could not include a unified guarantee of robust or exponential input-to-state stability under external forces. Especially, there is no human-robot interaction strategy of unilateral cable constraints. This paper presents a human-robot contact aware rapidly exponentially input-to-state stable control Lyapunov function (RES-ISS-CLF) based controller design for CDPRs, coupled with a QP-based tension distribution algorithm that executes a smooth, detection-triggered tension-reduction method to mitigate human–cable collisions, all evaluated in a wrapping simulator where a fixed cylinder emulates an arm-like obstacle. The stability of the system interacting with a human is guaranteed under the external wrenches and gravitational wrenches. The QP layer enforces unilateral cable constraints and allocates tensions during collision and recovery. The contributions of the paper are given as follows:

- A human-robot collision-aware constraint-based RES–ISS–CLF control of the CDPR provides exponential stability guarantees under unilateral cable constraints.
- A collision-time tension-management strategy that reduces contact loads while preserving trackability and avoiding oscillatory transients.

The remainder of this paper is organized as follows. Section II presents the system overview and simulation setup, detailing the control architecture and the collision/wrap simulator with the pick-and-place task. Section III formulates the problem and preliminaries, derives the CDPR model, and develops the collision-aware RES–ISS–CLF–QP controller under unilateral cable constraints. Section IV reports simulation results on cylinder-wrapping scenarios and compares against a PID–QP baseline. Section V concludes and outlines directions for future work.

II. System Overview and Simulation Setup

A. Control Architecture

Figure 2 depicts the overall scheme. *Black* blocks form the nominal pipeline that commands cable tensions $\boldsymbol{\tau}$ to realise the desired pose $\mathbf{p}_d$, twist $\mathbf{v}_d$, and twist rate $\dot{\mathbf{v}}_d$. *Red* blocks implement the collision–time tension–reduction policy layered on top of the nominal controller.

The collision management follows the sequential upper–bound reduction used in [17]. Upon detection of a collision time t_{col} and identification of the involved cable c, a smooth time vector $s(t)$ with a $1\,\mathrm{s}$ transition is activated to avoid abrupt tension changes. Let $\mathbf{SI} \in \mathbb{R}^{m\times m}$ be a selector (diagonal) matrix that isolates the collided cable; the management matrix is

$$\mathbf{S}(t) \;=\; s(t)\cdot \mathbf{SI}.$$

This schedule contracts the time-varying upper bounds element-wise, until the collided cable reaches its minimum allowable tension $\boldsymbol{\tau}_{\min}$. The bounds are fed to the tension–distribution (allocation) step, which, following [15], [17]–[19], solves

$$\begin{aligned} &\underset{\boldsymbol{\tau}}{\text{minimise}} \quad \|\boldsymbol{\tau}\|^2, \\ &\text{subject to} \quad \boldsymbol{\tau}_{\min} \le \boldsymbol{\tau} \le (\mathbf{I}-\mathbf{S}(t))\boldsymbol{\tau}_{\max}. \end{aligned} \tag{1}$$

The proposed RES–ISS–CLF–QP block computes the stabilizing platform command $\mathbf{u}^\star$ (see (17)), and the allocator maps $\mathbf{u}^\star$ to feasible tensions under the time-varying bounds.

B. Collision/Wrap Simulator

The CRAFT platform at LS2N is an eight-cable suspended CDPR. Each actuation chain comprises a motor with integrated gearbox, a winch, and a cable end at the MP attachment point A_i (see Fig. 1). In this study, A simulator is developed using the same nominal parameters as the hardware, accounting for pulley geometry and full rigid-body CDPR dynamics. Control is executed in Cartesian space: inputs are tensions $\boldsymbol{\tau}$; outputs are platform pose $(\mathbf{p},\boldsymbol{\theta})$, velocities $(\mathbf{v},\boldsymbol{\omega})$, and cable lengths. The plant dynamics are integrated at 100 Hz and the controller (RES–ISS–CLF–QP and tension-allocation QP) runs at 50 Hz. Cables are modeled as inelastic and massless.

Modeling of Human–Cable Collision. Cable–human interaction (arm, neck, or leg) is represented as wrapping about a fixed cylinder located within the feasible workspace so that collided-cable tensions remain manageable. Upon contact, the cable route between the MP anchor B_i and the pulley exit A_i is split by two contact points C_i (near A_i) and D_i (near B_i, see Fig. 3). For quasi-static trajectories (no sliding) [16], the incoming and outgoing segments are tangent to the cylinder at C_i and D_i. Denoting by $\vec{\mathbf{t}}(\cdot)$ the unit tangent on the cylinder surface at arc-length parameters s_c and s_d, the geometric constraints read

$$\begin{aligned} \vec{\mathbf{t}}(s_c) \parallel \overrightarrow{A_iC_i}, \\ \vec{\mathbf{t}}(s_d) \parallel \overrightarrow{B_iD_i}. \end{aligned} \tag{2}$$

Enforcing (2) updates the effective cable lengths and directions, from which the simulator computes the cable displacement. The controllers (proposed and baseline) require only the *collision-onset* flag to trigger the time-varying tension caps and do not use detailed contact geometry, preserving method generality to other convex obstacles.

Reference trajectory. The reference motion is a three-segment pick-and-place path using minimum-jerk profiles between way-points, following [22], which yields smooth transitions and efficient point-to-point motion.

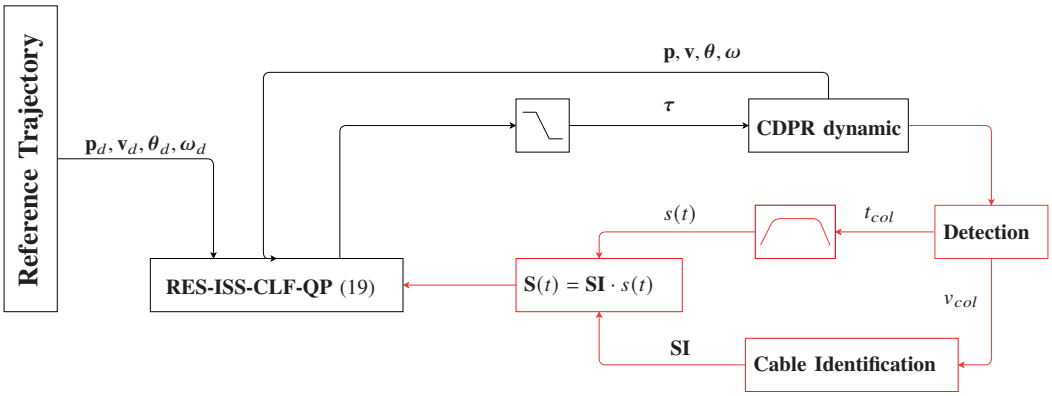

Fig. 2. Control scheme. Black: nominal RES–ISS–CLF–QP tracking with tension allocation. Red: collision management (detection, cable identification, and time-varying upper–bound reduction).

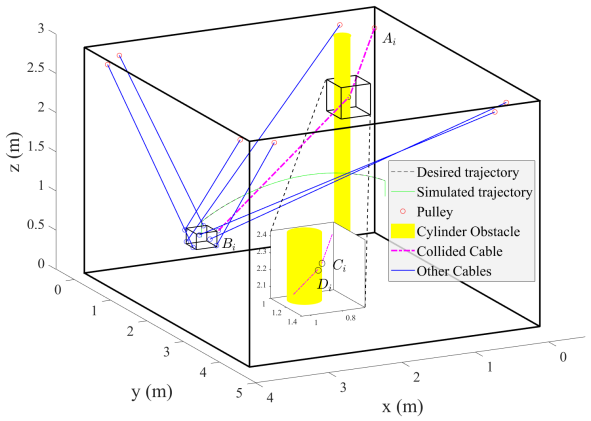

Fig. 3. Simulator with a fixed cylindrical obstacle. Cable i wraps around the cylinder, introducing two contact points C_i and D_i that split the route between the pulley exit A_i and the MP anchor B_i. In the quasi-static (no-slip) case, the entry/exit segments are tangent at C_i and D_i, enabling an updated computation of the cable displacement and cable lengths.

III. Problem Formulation

This section covers the problem definition, modeling of a CDPR, constraining the control input method when a cable-obstacle contact occurs, and a RES-ISS-CLF-based control law, which is proposed to solve the problem.

A. Preliminaries

Through the paper, the symbol $(\cdot)^\top$ represents the transpose of a vector and $(\cdot)^{-1}$ represents the inverse of a matrix. The output set is denoted by $\mathcal{Y} \subset \mathbb{R}^r$ and the input set is denoted by $\mathcal{U} \subset \mathbb{R}^m$. For clarity, the time dependence, t, of the equation is omitted if it is not necessary.

B. Problem Definition

The paper addresses the control problem, which guarantees the stability of the CDPR in the event of a cable-obstacle contact or collision, ensuring that the tracking error in Cartesian space is under a certain error value, and constraining the cable tensions within safe limits. The goal is to ensure the input-to-state stability of the CDPR, where at least one of the cable contacts a cylindrical obstacle. To address such a problem, a quadratic programming-based control method is proposed. The total wrench transmitted by the cables to the platform is constrained with a time-varying upper bound for safety reasons at the moments of contact. The method guarantees exponential convergence of the error to an equivalent point and ultimate boundedness against external wrenches under a cable-obstacle collision.

C. Modeling of the Cable-Driven Parallel Robot

In this subsection, the dynamic model of a CDPR is addressed based on the nonlinear control-affine structure obtained when cable tensions are selected as control inputs. The model is built using a full spatial representation that includes both position and orientation dynamics. A CDPR is presented in Fig. 1, where the platform is moved with m number of cables. The position of the platform is defined by $\mathbf{p} = [x\ y\ z]^\top$ and its orientation is defined by $\boldsymbol{\theta} = [\phi\ \vartheta\ \psi]^\top$. The orientation is transformed to the world coordinate system by the transformation matrix, which corresponds to the Euler angles ZYX. The dynamic equation of the CDPR is given by

$$\mathbf{W}(\mathbf{p}, \boldsymbol{\theta})\boldsymbol{\tau} + \mathbf{w}_e + \mathbf{w}_g - \mathbf{I}_s(\boldsymbol{\theta})\dot{\mathbf{v}} - \mathbf{C}(\boldsymbol{\theta}, \boldsymbol{\omega}) = 0, \qquad (3)$$

where $\tau \in \mathbb{R}^m$ is the cable tension, $m = 8$ is the total number of the cables, $\mathbf{I}_s(\boldsymbol{\theta}) \in \mathbb{R}^{6\times6}$ is the spatial inertia matrix, $\mathbf{C}(\boldsymbol{\theta}, \boldsymbol{\omega}) \in \mathbb{R}^6$ is the Coriolis and centrifugal components, $\mathbf{w}_e \in \mathbb{R}^6$ is the external wrench (e.g., direct interactions or field and environment loads on the MP), $\mathbf{w}_g = [\,0\ 0\ -m_g g\ 0\ 0\ 0\,]^\top \in \mathbb{R}^6$ is the gravitational wrench, m_g is the platform mass, and g is equal to $g = 9.81\,\mathrm{m\,s^{-2}}$ [23]. Note that the dynamics (3) can be represented in terms of the state $\mathbf{x} := [\mathbf{p}\ \boldsymbol{\theta}\ \mathbf{v}\ \boldsymbol{\omega}]^\top \in \mathbb{R}^{12}$ as

$$\dot{\mathbf{x}} = \underbrace{\begin{bmatrix} \mathbf{v} \\ T(\boldsymbol{\theta})\boldsymbol{\omega} \\ -\mathbf{I}_s^{-1}\mathbf{C}(\boldsymbol{\theta}, \boldsymbol{\omega}) \end{bmatrix}}_{f(\mathbf{x})} + \underbrace{\begin{bmatrix} 0_{3\times8} \\ 0_{3\times8} \\ \mathbf{I}_s^{-1}\mathbf{W}(p, \boldsymbol{\theta}) \end{bmatrix}}_{g(\mathbf{x})} + \underbrace{\begin{bmatrix} 0_{3\times8} \\ 0_{3\times8} \\ \mathbf{I}_s^{-1}\mathbf{w}_{eg} \end{bmatrix}}_{d(\mathbf{x})},$$

where $\mathbf{v} = \dot{\mathbf{p}}$ is the translational velocity vector, and $\boldsymbol{\omega}$ is the angular velocity vector, $T(\boldsymbol{\theta})$ is the Euler kinematics,

and $\mathbf{w}_{eg} = \mathbf{w}_e + \mathbf{w}_g$. Here, $d(\mathbf{x})$ defines the effects of the external and gravitational wrenches on the cables.

Assumption 3.1: (Bounded disturbance) The disturbance d is assumed to be an unknown function but predictable and norm-bounded as

$$||d||_\infty := \sup_{t\geq 0} \|d(t)\| < \overline{d}. \tag{4}$$

Let the $\mathbf{y} = h(\mathbf{x}) = [\mathbf{p} \quad T(\boldsymbol{\theta})\boldsymbol{\omega}]^\top$ be the output function, then the relative degree r is defined by

$$\begin{aligned} &L_g L_f^{i-1} h = 0, \quad i = 1, 2, \ldots, r-1, \\ &L_g L_f^{r-1} h \neq 0, \end{aligned} \tag{5}$$

where $L_f h$ and $L_f h$ are the Lie derivatives of h in the directions of f and g, respectively.

Definition 3.1: [24] A CLF on the output dynamics for the system in (3) assuming $d \triangleq 0$ and the set of allowed internal dynamics is a continuously differentiable function V satisfying the following

$$\begin{aligned} &c_1\|\mathbf{x}\| \;\leq\; V(\mathbf{x}) \;\leq\; c_2\|\mathbf{x}\|, \\ &\inf_{\mathbf{u}\in\mathbb{R}^m} \; \big[L_f V(\mathbf{x}) + L_g V(\mathbf{x})\,\mathbf{u}\big] \leq -c_3 V(\mathbf{x}), \end{aligned} \tag{6}$$

for positive scalars $c_1,\ c_2,\ c_3 \in \mathbb{R}_{>0}$. The equation (6) highlights that exponential stability of the nominal system in (3) is guaranteed if the conditions are satisfied [24]. Then the CLF-QP controller is structured as

$$\begin{aligned} \mathbf{u} &= \arg\min_{\mathbf{u}\in\mathbb{R}^m} ||\mathbf{u}||^2 \\ \text{s.t.} \quad & L_f V(\mathbf{x}) + L_g V(\mathbf{x})\mathbf{u} \leq -c_3 V(\mathbf{x}) \\ & \mathbf{u}_{min} \leq \mathbf{u} \leq \mathbf{u}_{max}. \end{aligned}$$

In case of collision between a human or an obstacle with the CDPR or putting on additional mass on the platform, the CLF-controlled closed-loop system (3) may not maintain the system stability. An input-to-state stabilizing control Lyapunov function (ISS-CLF) can render the stability under such conditions.

Definition 3.2: [25] A continuously differentiable function V is a rapidly exponentially stabilizing ISS-CLF function satisfying

$$\begin{aligned} &c_1\|\mathbf{x}\|^2 \leq V(\mathbf{x}) \leq \frac{c_2}{\varepsilon^2}\|\mathbf{x}\|^2 \\ &L_f V(\mathbf{x}) + L_g V(\mathbf{x})\mathbf{u} \leq -\frac{c_3}{\varepsilon} V(\mathbf{x}) + \frac{1}{\overline{\varepsilon}}||d||^2, \end{aligned} \tag{7}$$

for ε, a positive scalar within $(0, 1)$, $\overline{\varepsilon}$ is also a positive scalar, and c_{1-3} are positive scalars.

D. Designing collision aware RES-ISS-CLF-QP controller for the CDPR

The Lyapunov function-based stability analysis is widely preferred to analyze or synthesize controllers in nonlinear systems. However, finding a valid Lyapunov function is a challenging task for a nonlinear control-affine system in (3). In linear systems, there is a necessary condition for finding a valid Lyapunov function. For a linear system $\dot{\mathbf{x}} = \mathbf{A}_{cl}\mathbf{x}$, a valid Lyapunov function can be found

$$V(\mathbf{x}) = \mathbf{x}^\top \mathbf{P} \mathbf{x}, \tag{8}$$

which satisfy

$$\dot{V}(\mathbf{x}) = \mathbf{x}^\top (\mathbf{A}_{cl}^\top \mathbf{P} + \mathbf{P}\mathbf{A}_{cl})\mathbf{x} \preceq 0. \tag{9}$$

where $\mathbf{P} = \mathbf{P}^\top > 0$ is a positive definite matrix and $\mathbf{A} \in \mathbb{R}^{n\times n}$ is Hurwitz square matrix. Assume that there is a solution such that

$$\mathbf{A}_{cl}^\top \mathbf{P} + \mathbf{P}\mathbf{A}_{cl} \preceq -\mathbf{Q}, \tag{10}$$

then (8) is a valid choice for the linear system that maintains the origin is globally stable [26]. The equation (10) defines a linear matrix inequality (LMI) which can be solved using numerically efficient solvers, i.e., $sedumi$ and $mosek$ etc. To find a valid Lyapunov function, assume there exists a diffeomorphism $((\eta, z) = \Phi(x))$ that results in the normal form representation [27]

$$\begin{aligned} \dot{\eta} &= \mathbf{F}(\eta, \mathbf{z}) + \mathbf{G}(\eta, \mathbf{z})\mathbf{b} \\ \dot{\mathbf{z}} &= h_v(\eta, \mathbf{z}), \end{aligned} \tag{11}$$

where $\eta \in Y \subset \mathbb{R}^r$ is the output dynamics of the original system, $\mathbf{b} \subseteq \mathbb{R}^m$ is the virtual control input, $\mathbf{z} \in Z \subset \mathbf{R}^{n-r}$ is the zero dynamics. The input to output linear system is obtained by taking the derivative of the output equation. The second derivative of the output equation is given by

$$\begin{aligned} \ddot{\mathbf{y}} = &\underbrace{\begin{bmatrix} \frac{1}{m_g}\mathbf{0}_3 \\ \dot{T}(\boldsymbol{\theta},\boldsymbol{\omega})\,\boldsymbol{\omega} \;-\; T(\boldsymbol{\theta})\,\mathbf{I}_s^{-1}\big(\boldsymbol{\omega}\times(\mathbf{I}_s\boldsymbol{\omega})\big) \end{bmatrix}}_{\mathbf{F}_p(\mathbf{x})} \\ &+ \underbrace{\begin{bmatrix} \frac{1}{m_g}\mathbf{U}(p,\boldsymbol{\theta}) \\ T(\boldsymbol{\theta})\,\mathbf{I}_s^{-1}\,\mathbf{M}(p,\boldsymbol{\theta}) \end{bmatrix}}_{\mathbf{G}_p(\mathbf{x})}\mathbf{u} + \underbrace{\begin{bmatrix} \frac{1}{m_g}\mathbf{F}_t \\ T(\boldsymbol{\theta})\,\mathbf{I}_s^{-1}\,\mathbf{F}_r \end{bmatrix}}_{\mathbf{d}_{\ddot{y}}(\mathbf{x})}, \end{aligned} \tag{12}$$

where $\mathbf{U}(p, \boldsymbol{\theta}) \in \mathbf{R}^{3\times 8}$ is the transitional part of the wrench matrix, $\mathbf{M}(p, \boldsymbol{\theta}) \in \mathbf{R}^{3\times 8}$ is the rotational part of the wrench matrix, $\mathbf{F}_t = \mathbf{F}_e + \mathbf{F}_g \in \mathbf{R}^3$ is the transitional part of the matrix $(\mathbf{w}_{eg})$, $\mathbf{F}_r = -\boldsymbol{\omega} \times (\mathbf{I}_s\boldsymbol{\omega}) + \mathbf{T}_e + \mathbf{T}_g \in \mathbf{R}^3$ is the rotational part of the matrix $(\mathbf{w}_{eg})$, $\mathbf{G}_p(\mathbf{x}) \in \mathbf{R}^{6\times 8}$, and the scaled disturbance $||\mathbf{d}_{\ddot{y}}(t)||$ is bounded with $\overline{d}_y$ for $\forall t \geq 0$. We have reached the input vector in the second derivative of the output vector. The system is fully feedback linearizable (no zero dynamics) since the relative degree vector is found as $r = [2\ 2\ 2\ 2\ 2\ 2]$. Define a canonical linear chain

$$\dot{\eta} = \mathbf{F}\eta + \mathbf{G}\mathbf{b}, \quad \mathbf{F} = \begin{bmatrix} 0_{6\times 6} & I_{6\times 6} \\ 0_{6\times 6} & 0_{6\times 6} \end{bmatrix},\ \mathbf{G} = \begin{bmatrix} 0_{6\times 6} \\ I_{6\times 6} \end{bmatrix}, \tag{13}$$

where

$$\dot{\eta} = \begin{bmatrix} \dot{\mathbf{e}} \\ \ddot{\mathbf{e}} \end{bmatrix} = \begin{bmatrix} 0_{6\times 6} & I_{6\times 6} \\ 0_{6\times 6} & 0_{6\times 6} \end{bmatrix} \begin{bmatrix} \mathbf{e} \\ \dot{\mathbf{e}} \end{bmatrix} + \begin{bmatrix} 0_{6\times 6} \\ I_{6\times 6} \end{bmatrix} \mathbf{b}, \tag{14}$$

then $\mathbf{b} = \ddot{\mathbf{y}} - \ddot{\mathbf{y}}_d$, where The matrix $\mathbf{F}$ is not Hurwitz; therefore, an additional vector should be defined using a state-feedback control law $(\mathbf{b} = -\mathbf{K}\eta)$. To ensure $\mathbf{F}$ matrix is a Hurwitz one, the Continuous-Time Algebraic Riccati Equation (CARE) is defined as

$$\mathbf{F}^\top \mathbf{P} + \mathbf{P}\mathbf{F} - \mathbf{P}\mathbf{G}\mathbf{G}^\top \mathbf{P} \preceq -\mathbf{Q}. \tag{15}$$

The control law is constructed using the solution of (15) as $\mathbf{K} = -\frac{1}{2}\mathbf{G}^\top\mathbf{P}\eta$. Consider (11), and assume that there exist a controller $\mathbf{b} = -\mathbf{K}\eta$ can make the closed-loop system $\dot{\eta} = \mathbf{A}_{cl}\eta = (\mathbf{F} - \mathbf{G}\mathbf{K})\eta$ is Hurwitz. Then the Lyapunov function, $V(\eta) = \eta^\top\mathbf{P}\eta$, is a valid control Lyapunov function satisfying

$$\lambda_{\min}(\mathbf{P})\|\eta\|^2 \leq V(\eta) \leq \lambda_{\max}(\mathbf{P})\|\eta\|^2$$
$$\inf_{b\in\mathbb{R}^m}[L_F V(\eta) + L_G V(\eta)\mathbf{b}] \leq -\frac{\lambda_{\min}(\mathbf{Q})}{\lambda_{\max}(\mathbf{P})}V(\eta), \quad (16)$$

for a positive definite matrices $\mathbf{P} = \mathbf{P}^\top > 0$ and $\mathbf{Q} = \mathbf{Q}^\top > 0$ by solving the (15). The terms $\lambda_{min}(\cdot)$ and $\lambda_{max}(\cdot)$ define min and max eigenvalues of a matrix. Following $\mathbf{b} = \mathbf{F_p}(\mathbf{x}) + \mathbf{G_p}(\mathbf{x})\mathbf{u} - \ddot{\mathbf{y}}_d$ and considering (11), the control law is re-structured as

$$\mathbf{u}^* = \arg\min_{u\in\mathbb{R}^m} ||\mathbf{F_p}(\mathbf{x}) + \mathbf{G_p}(\mathbf{x})\mathbf{u} - \ddot{\mathbf{y}}_d||^2 \quad (17)$$
$$\text{s.t.} \quad \eta^\top(\mathbf{F}^\top\mathbf{P} + \mathbf{P}\mathbf{F})\eta + 2\eta^\top\mathbf{P}\mathbf{G}(\mathbf{G_p}(\mathbf{x})\mathbf{u} + \mathbf{F_p}(\mathbf{x}) - \ddot{\mathbf{y}}_d)$$
$$\leq -\frac{\lambda_{min}(\mathbf{Q})}{\lambda_{max}(\mathbf{P})}V_\varepsilon(\eta) + \frac{1}{\bar{\varepsilon}}||2\eta^\top\mathbf{P}\mathbf{G}||^2$$
$$\mathbf{u}_{min} \leq \mathbf{u} \leq \mathbf{u}_{max}$$

where $V_\varepsilon(\eta) = \eta^\top\mathbf{P}_\varepsilon\eta$ and $\mathbf{P}_\varepsilon = \mathbf{P}/\varepsilon$. The equation ensures the stability of (3) under a human-robot interaction or uncertainties of the platform mass when the slack variable becomes zero. However, there is no management method in (17) in case of human-cable interaction which may deteriorates the system tracking and stability conditions. Following [18], the RES-ISS-CLF-QP controller is combined with the tension management strategy as

$$\mathbf{u}^* = \arg\min_{u\in\mathbb{R}^m} ||\mathbf{F_p}(\mathbf{x}) + \mathbf{G_p}(\mathbf{x})\mathbf{u} - \ddot{\mathbf{y}}_d||^2 \quad (18)$$
$$\text{s.t.} \quad \eta^\top(\mathbf{F}^\top\mathbf{P} + \mathbf{P}\mathbf{F})\eta + 2\eta^\top\mathbf{P}\mathbf{G}(\mathbf{G_p}(\mathbf{x})\mathbf{u} + \mathbf{F_p}(\mathbf{x}) - \ddot{\mathbf{y}}_d)$$
$$\leq -\frac{\lambda_{min}(\mathbf{Q})}{\lambda_{max}(\mathbf{P})}V_\varepsilon(\eta) + \frac{1}{\bar{\varepsilon}}||2\eta^\top\mathbf{P}\mathbf{G}||^2$$
$$\mathbf{u}_{\min} \leq \mathbf{u} \leq (\mathbf{I} - \mathbf{S}(t))\mathbf{u}_{\max}.$$

IV. Results and Analysis

This section covers the simulation results of the proposed human-cable collision management strategy of the CDPR. A desired trajectory is defined as in Fig. 4 to demonstrate the tracking performance of the CDPR in the case of the human-cable interaction, where the human is modeled as a cylinder. The interaction is applied to the second cable of the system when the closed-controlled system follows the desired trajectory. The objective of the system is to maintain its tracking performance smoothly after interaction occurs. The configuration of the control system is presented in Fig. 4, where the interaction occurs at half the time of the simulation setup. The simulation is constructed in the MATLAB environment, (15) is solved using *care* solver, and the QP problem is solved using *quadprog* solver. The term ε is chosen as 0.5, $\bar{\varepsilon}$ is chosen as 1.7, and the matrix $\mathbf{Q}$ is chosen $25\mathbf{I}$ to design RES-ISS-CLF controller. The time-varying upper bounds of the cable tensions are presented

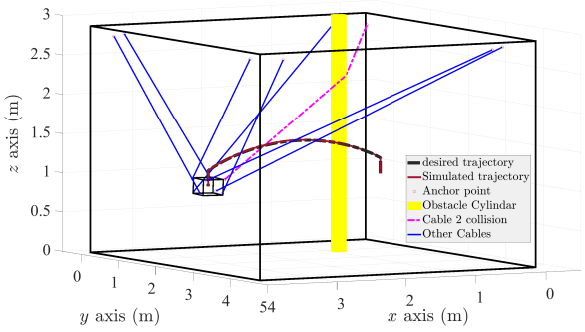

Fig. 4. The closed-loop controlled system of the CDPR, which has the trajectory tracking and the human-cable collision management objectives

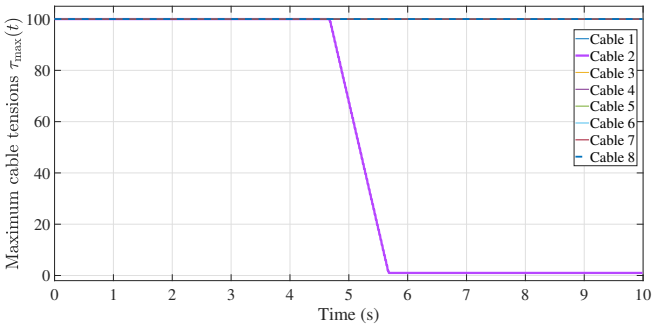

Fig. 5. The time-varying upper bound of the second cable tension: the changing of the cable 2 in case of interaction with an obstacle versus time

in Fig. 5, where the second cable makes contact with the obstacle at 4.56 seconds. The time-varying bound of the cable is decreased as in (1). A PID controller and a nominal CLF controller are designed to compare the performance of the proposed control law. Tracking performance of the control laws are presented in Fig. 6. The control laws with the proposed management strategy maintain the trajectory performances; however, the PID-controlled system without any management strategy could not maintain the tracking performance. The errors of the RES-ISS-CLF controlled closed-loop control system with the management strategy is presented in Fig. 7. The cable tensions of the control laws are presented in Fig. 8, where the effect of the interaction on cable 2 is presented. The proposed control law mitigates the chattering in the control inputs in case any human-robot interactions. The law achieves the control objectives using slightly lower control efforts.

To demonstrate the stability guarantee of the proposed control law, the Lyapunov function of the CLF-controlled closed-loop systems are presented in Fig. 9. The nominal CLF-QP controlled system could not mitigate the dramatic increase in the function at the moment of contact. The RES-ISS-CLF controlled system achieve the limit the increase of the function and rapidly exponential decrease of the function. The functions are continuously differentiable and bounded in all operating times. To demonstrate the performance of the RES-ISS-CLF-QP law, the $\dot{V}_{CLF}$, which is given left-hand side (LHS) of the stability constraint of (17) is presented in Fig. 10. The control law dramatically increases the decay

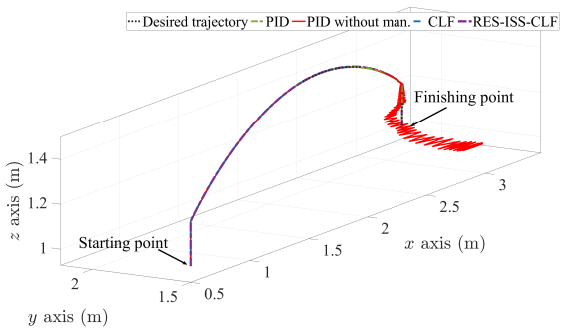

Fig. 6. The tracking performance of the control laws under human-obstacle interaction occurring at time $t = 4.56$ seconds (management=man)

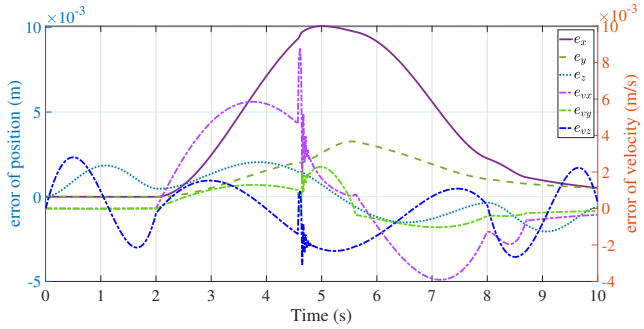

Fig. 7. The errors of the RES-ISS-CLF controlled system with the management strategy versus time

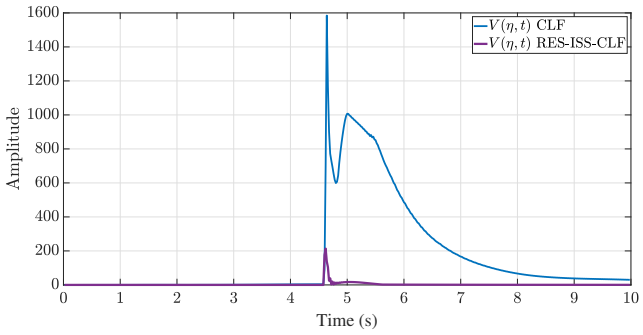

Fig. 9. The Lyapunov functions of the control laws versus time in case of human-cable interaction

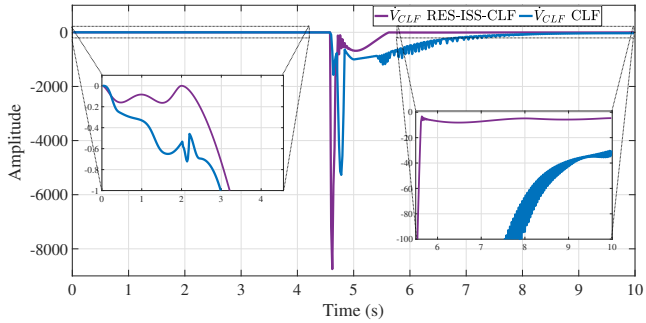

Fig. 10. The trajectory of the Lyapunov functions, which is defined on the left-hand side of the CLF constraints versus time

rate of the Lyapunov function to obtain a rapid exponential convergence to the desired equivalent point. To ensure system stability during nominal operation, even during and after human-robot contact, the functions continue to take negative values. The reason the values are close to zero in nominal operation is the low steady-state error.

V. Conclusion

This work presented a RES–ISS–CLF–QP control framework for CDPRs operating under human–cable interaction. The design combines a rapid–exponential CLF for output tracking with an ISS bound to exogenous contact wrenches, and a QP-based tension allocator that enforces unilateral cable constraints. A tension distribution algorithm reduces cable upper bounds smoothly, mitigating collision without large oscillations. Using a wrapping simulator with a fixed cylindrical obstacle, the approach achieved tighter tracking, reduced overshoot and oscillation, fewer tension-bound violations, and lower peak contact loads than a PID–QP baseline, while maintaining real-time solve rates.

The study assumed known geometry, inelastic massless cables, and frictionless wrap. Next steps include (i) hardware validation on the CRAFT platform with sensing noise and latency, (ii) integration with compliance/trajectory shaping to further dissipate post-contact energy, and (iii) adaptive estimation of contact/disturbance bounds to tighten ISS margins. Extending the formulation to nonconvex obstacles and broader pHRI tasks is also of interest.

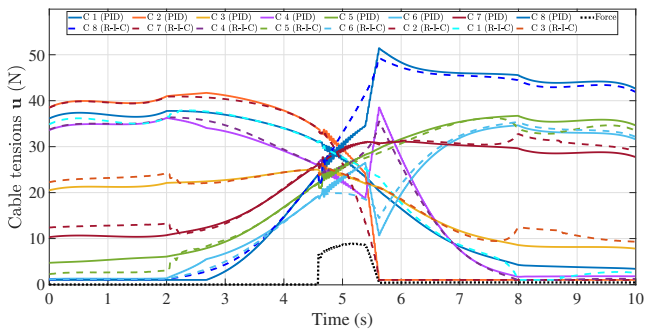

Fig. 8. The cable tensions of the PID and RES-ISS-CLF controlled control systems (Cable=C) and (RES-ISS-CLF=R-I-C)

Acknowledgments

This work was supported by ROBOTEX 2.0 (ANR-10-EQPX-44-01), TIRREX (ANR-21-ESRE-0015), Titanbot (ANR-23-DMRO-0020), and by the Agence Nationale de la Recherche under the France 2030 program (PEPR O2R–AS1, ANR-22-EXOD-0005). The second author is funded by the China Scholarship Council (Grant no. 202208070012).

References

[1] A. Pott and T. Bruckmann, *Cable-driven parallel robots*. Springer, 2013, vol. 116.

[2] Z. Zhang, Z. Shao, and L. Wang, "Optimization and implementation of a high-speed 3-dofs translational cable-driven parallel robot," *Mechanism and Machine Theory*, vol. 145, p. 103693, 2020.

[3] S. Qian, B. Zi, W.-W. Shang, and Q.-S. Xu, "A review on cable-driven parallel robots," *Chinese Journal of Mechanical Engineering*, vol. 31, no. 1, pp. 1–11, 2018.

[4] J. Garrido, D. Silva-Muñiz, E. Riveiro, J. Rivera-Andrade, and J. Sáez, "Collaborative behavior for non-conventional custom-made robotics: A cable-driven parallel robot application," *Machines*, vol. 12, no. 2, 2024. [Online]. Available: https://www.mdpi.com/2075-1702/12/2/91

[5] H. Mahnke and R. J. Caverly, "Fast and reliable iterative cable-driven parallel robot forward kinematics: A quadratic approximation approach," in *International Conference on Cable-Driven Parallel Robots*. Springer, 2025, pp. 3–15.

[6] V. L. Nguyen and R. J. Caverly, "Cable-driven parallel robot pose estimation using extended kalman filtering with inertial payload measurements," *IEEE Robotics and Automation Letters*, vol. 6, no. 2, pp. 3615–3622, 2021.

[7] F. Zhang, W. Shang, G. Li *et al.*, "Calibration of geometric parameters and error compensation of non-geometric parameters for cable-driven parallel robots," *Mechatronics*, vol. 77, 2021.

[8] S. Baklouti, E. Courteille, S. Caro *et al.*, "Dynamic and oscillatory motions of cable-driven parallel robots based on a nonlinear cable tension model," *Journal of Mechanisms and Robotics*, vol. 9, no. 6, p. 061014, 2017.

[9] J.-P. Merlet, "Estimating the young modulus of cables material in cable-driven parallel robots," in *International Conference on Cable-Driven Parallel Robots*. Springer, 2025, pp. 28–40.

[10] H. Ji, W. Shang, and S. Cong, "Adaptive synchronization control of cable-driven parallel robots with uncertain kinematics and dynamics," *IEEE Transactions on Industrial Electronics*, vol. 68, no. 9, pp. 8444–8454, 2021.

[11] M. Zeinali and A. Khajepour, "Design and application of chattering-free sliding mode controller to cable-driven parallel robot manipulator: Theory and experiment," in *ASME 2010 International Design Engineering Technical Conferences and Computers and Information in Engineering Conference*, 2010, pp. 319–327.

[12] H. J. Asl and F. Janabi-Sharifi, "Adaptive neural network control of cable-driven parallel robots with input saturation," *Engineering Applications of Artificial Intelligence*, vol. 65, pp. 252–260, 2017.

[13] Y. Lu, C. Wu, W. Yao *et al.*, "Deep reinforcement learning control of fully-constrained cable-driven parallel robots," *IEEE Transactions on Industrial Electronics*, vol. 70, no. 7, pp. 7194–7204, 2023.

[14] J. C. Santos, M. Gouttefarde, and A. Chemori, "A nonlinear model predictive control for the position tracking of cable-driven parallel robots," *IEEE Transactions on Robotics*, vol. 38, no. 4, pp. 2597–2616, 2022.

[15] T. Rousseau, C. Chevallereau, and S. Caro, "Human-cable collision detection with a cable-driven parallel robot," *Mechatronics*, vol. 86, p. 102850, 2022.

[16] H. Xiong and Y. Xu, "Statics and path of the cables of a cable-driven parallel robot wrapping on surfaces," in *International Conference on Cable-Driven Parallel Robots*. Springer, 2023, pp. 82–94.

[17] H. Gao, C. Chevallereau, and S. Caro, "Detection and management of human-cable collision in cable-driven parallel robots," *IEEE Robotics and Automation Letters*, vol. 9, no. 12, pp. 11 698–11 705, 2024.

[18] ——, "Advancements in human-cable collision detection and management in cable-driven parallel robots," in *Cable-Driven Parallel Robots*, D. Lau, A. Pott, and T. Bruckmann, Eds. Cham: Springer Nature Switzerland, 2025, pp. 246–258.

[19] ——, "Enhancing safety in collaborative cable-driven parallel robots: Contact distinction and management for carrying tasks," *IEEE Transactions on Automation Science and Engineering*, vol. 22, pp. 18 860–18 874, 2025.

[20] J. Jang, M. Zhao, and T. Bewley, "A control lyapunov function-based quadratic program for the cable-driven boat motion simulator," in *2022 7th International Conference on Robotics and Automation Engineering (ICRAE)*, 2022, pp. 18–24.

[21] B. Zhang, W. Shang, and S. Cong, "Synchronous impedance control of cable-driven parallel robots with external interaction," *IEEE/ASME Transactions on Mechatronics*, pp. 1–13, 2025.

[22] E. Picard, S. Caro, F. Plestan, and F. Claveau, "Control solution for a cable-driven parallel robot with highly variable payload," in *International Design Engineering Technical Conferences and Computers and Information in Engineering Conference*, vol. 51814. American Society of Mechanical Engineers, 2018, p. V05BT07A013.

[23] L. Gagliardini, M. Gouttefarde, and S. Caro, "Determination of a dynamic feasible workspace for cable-driven parallel robots," *Advances in Robot Kinematics 2016*, pp. 361–370, 2018.

[24] W. D. Compton, I. D. J. Rodriguez, N. Csomay-Shanklin, Y. Yue, and A. D. Ames, "Constructive nonlinear control of underactuated systems via zero dynamics policies," in *2024 IEEE 63rd Conference on Decision and Control (CDC)*. IEEE, 2024, pp. 8350–8357.

[25] S. Kolathaya, J. Reher, A. Hereid, and A. D. Ames, "Input to state stabilizing control lyapunov functions for robust bipedal robotic locomotion," in *2018 Annual American Control Conference (ACC)*. IEEE, 2018, pp. 2224–2230.

[26] R. Tedrake, "Underactuated robotics: Learning, planning, and control for efficient and agile machines course notes for mit 6.832," *Working draft edition*, vol. 3, no. 4, p. 2, 2009.

[27] A. Isidori, *Nonlinear control systems: an introduction*. Springer, 1985.